Carbazole-Based Hole-Transport Materials for Efficient Solid-State Dye-Sensitized Solar Cells and Perovskite Solar Cells

*Bo Xu, Esmaeil Sheibani, Peng Liu, Jinbao Zhang, Haining Tian, Nick Vlachopoulos, Gerrit Boschloo, Lars Kloo, Anders Hagfeldt, and Licheng Sun**

With the recent rise in awareness of environmental and energy issues, renewable energy sources are given more and more attention. Looking at photovoltaics, dye-sensitized solar cell (DSC) is considered to be a promising candidate as a large-area and low-cost renewable energy source.[1] In this rapidly developing field, the identification of efficient electrolytes to improve efficiency is of great importance for the promotion of DSCs.[2,3] So far, the best conversion efficiency of 13% have been obtained with prophyrin-based dyes used together with the Co(II/III)-tris(bipyridyl) complexes as redox couple in liquid electrolytes.[4] Despite the fact that considerable progress has been made in this field of research, the risk of leakage associated with the volatile nature of a liquid electrolyte, together with fundamental stability issues represent significant limitations for the commercialization of these devices.[3] A significant part of the efforts made in this field has been devoted to the optimization of the fabrication of solar cells based on solid-state hole-transport materials (HTMs) as the formal electrolyte system responsible for the regeneration (reduction) of the sensitizing dye molecules.[5,6] To date, the highest efficiency reported amounts to 7.2% for solid-state dye-sensitized solar cells (ssDSCs)[7] and 15.4% for perovskite solar cells (PSCs);[8] both champion results have been achieved using Spiro-OMeTAD as the HTM. However, previous studies have demonstrated that the onerous synthesis[9] and low charge-carrier mobility[10] of Spiro-OMeTAD significantly limit its potential of up-scaling for applications of ssDSCs and PSCs.[11,12] Therefore, the development of a new generation of HTMs[13] with low cost, facile synthesis and high charge-carrier mobility is of high priority.[6,14] Carbazole-based derivatives have attracted much attention because of their interesting photochemical properties.[15] Recent interest in the carbazole derivatives has been caused by its good charge-transport function, which can be exploited in the molecular design of new types of HTMs in organic light-emitting diodes (OLED)[16] and as electron donor group in organic sensitizers of D-π-A-type in DSCs.[17] Another fascinating advantage is the versatility of the carbazole reactive sites that can be substituted with a wide variety of functional groups, allowing fine-tuning of its optical and electrical properties.[18] Herein, we present on the design and synthesis of two novel carbazole-based, small-molecule organic HTMs denoted **X51** and **X19** (**Figure 1**) characterized by a straightforward synthetic route and high hole mobility, together with their successful application in ssDSCs and PSCs. One of the HTM- based, **X51**, devices exhibit high power conversion efficiencies (PCEs) amounting to 6.0% and 9.8% in dye sensitized and perovskite solar cells, respectively. These results are comparable to the PCEs of 5.5% and 10.2% obtained by using the well-studied champion HTM, Spiro-OMeTAD, under standard AM 1.5 solar light illumination of 100 mW·cm^{-2} intensity. To the best of our knowledge, this is the first report of a carbazole-based, small-molecule organic HTM that can challenge the state-of-the-art HTM Spiro-OMeTAD both in ssDSCs and PSCs.

Results from DFT calculations give insights into the highest occupied molecular orbital (HOMO) and the lowest unoccupied molecular orbital (LUMO) of the HTMs, as are shown in Figure S1. The energies of the calculated HOMO and LUMO of these HTMs have been summarized in Table S1, and these data make it clear that the energy of the HOMO levels of all HTMs are very similar. The reorganization energy represents the relaxation of the molecule after oxidation or reduction, typically modeled by withdrawing or adding one electron, and a small reorganization energy implies, based on the anatomy of a Marcus-type electron-transfer mechanism between the molecules in the molecular HTMs, fast transfer rate for electrons or

B. Xu, Dr. E. Sheibani, Dr. H. Tian, Prof. L. Sun
Organic Chemistry
Center of Molecular Devices
Department of Chemistry
School of Chemical Science and Engineering
KTH Royal Institute of Technology
10044 Stockholm, Sweden
E-mail: lichengs@kth.se

P. Liu, Prof. L. Kloo
Applied Physical Chemistry
Center of Molecular Devices
Department of Chemistry
School of Chemical Science and Engineering
KTH Royal Institute of Technology
SE-10044 Stockholm, Sweden

J. Zhang, Dr. H. Tian, Dr. N. Vlachopoulos, Dr. G. Boschloo, Prof. A. Hagfeldt
Physical Chemistry
Department of Chemistry-Ångström Laboratory
Uppsala University
Box 523, SE-75120, Uppsala, Sweden

Prof. L. Sun
State Key Laboratory of Fine Chemicals
DUT-KTH Joint Research Centre on Molecular Devices
Dalian University of Technology (DUT)
116024 Dalian, China

DOI: 10.1002/adma.201402415

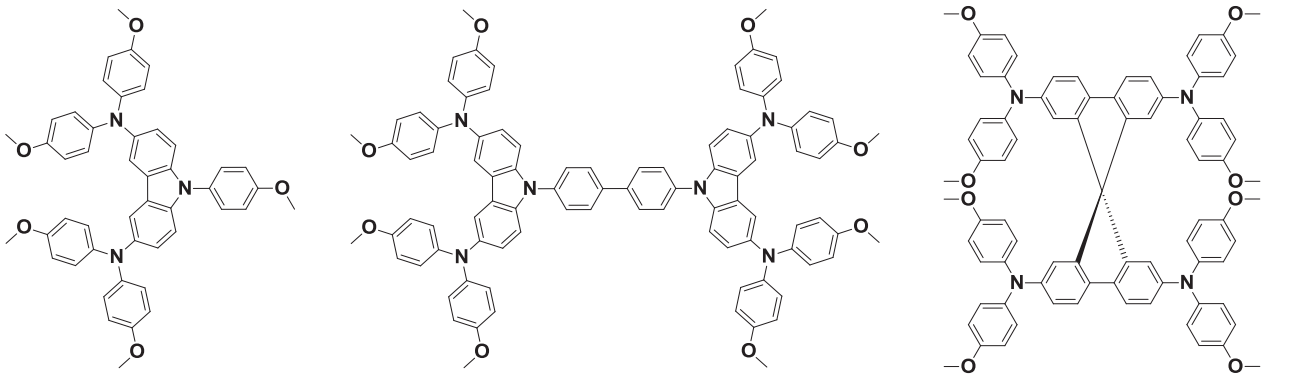

Figure 1. Molecular structures of HTM **X19**, **X51** and Spiro-OMeTAD; the molecular weights are given in g/mol.

holes. As indicated in **Table 1**, the molecule **X51** has the lowest calculated reorganization energy. This implies, on a relative scale, faster hole-transport than the other two HTMs. It is not unlikely that these properties can be assigned to the larger conjugation length of **X51 as** compared to Spiro-OMeTAD and **X19** from an intrinsic structural point of view.

The synthetic routes of **X19** and **X51** are shown in Scheme. S1. Inexpensive starting materials were utilized to synthesize the desired materials. **X19** was synthesized by a bromination, a copper-catalyzed Ullman reaction and a palladium-catalyzed Buchwald-Hartwig reaction step. Compared to **X19**, the synthesis of **X51** requires one further step of protection and deprotection. All of the materials were characterized by $^{1}H/^{13}C$ NMR spectroscopy and high-resolution mass spectrometry (HR-MS) (Figures S2–S7). The role of Spiro-OMeTAD is as a reference HTM in this study.

Cyclic Voltammetry (CV) (Figure S8) and Differential Pulsed Voltammetry (DPV) (**Figure 2**b) applied to each of the HTMs were recorded in order to determine the ground-state oxidation potential (E_{OX}). The corresponding data are collected in Table 1. The E_{OX} values were determined to 0.61 V and 0.64 V vs. NHE in DCM solution for **X19** and **X51**, respectively. Considering the oxidation potential (0.88V vs. NHE) of the LEG4 dye,[19] all hole conductors have an overpotential between 270 mV and 240 mV, which should be sufficient for efficient regeneration of the oxidized dye. The optical absorption and fluorescence spectra (Figure 2a) in DCM were recorded at a concentration of 10^{-5} M. All photophysical data of the HTMs are listed in Table 1. **X19** and **X51** exhibit strong absorption at 310 nm and a weak spectral feature at 370 nm, while the absorption of Spiro-OMeTAD shows a weak feature at 306 nm and strong absorption at 386 nm. The weak absorption in the visible light region indicates that all of these HTMs will not obstruct sunlight from efficiently reaching the sensitizing dye molecules. In addition, the photoluminescence spectra show that the X-type HTMs display an emission peak around 460 nm. This is slightly red-shifted as compared to Spiro-OMeTAD. From the intersection of the emission and absorption spectra we can obtain the E_{0-0} transition energy and thus estimate the optical band gap (Table 1).

As previously highlighted, charge transport is another significant parameter to consider in the design of new HTMs for ssDSCs. Herein, the hole mobility of the HTMs were determined by use of space-charge-limited currents (SCLCs) according to literature.[11,20] Fitting the *J–V* curves (Figure 2c) for each material to this expression gives the mobility data listed in Table 1. The value obtained here for Spiro-OMeTAD is similar to the data reported in the literature and our former work.[21] The hole mobility of **X51** is slightly higher than that of **X19**, and

Table 1. Summary of optical, electrochemical, photoelectrical properties and reorganization energy of the HTMs used in this study.

HTMs	λ_{abs} [nm]		λ_{em} [nm]	E_{ox} [a)] [V vs NHE]	E_{o-o} [b)] [eV]	E_R [c)] (meV)	Hole Mobility [d)] ($cm^2 \cdot V^{-1} \cdot s^{-1}$)	Conductivity [e)] ($S \cdot cm^{-1}$)
X19	310(max)	371	457	**0.61**	2.95	395	1.19×10^{-4}	2.88×10^{-5}
X51	307(max)	365	469	**0.64**	2.93	378	1.51×10^{-4}	1.05×10^{-4}
Spiro-OMeTAD	306	386(max)	423	**0.63**	3.05	495	5.31×10^{-5}	8.67×10^{-5}

[a)]0.1 M of tetrabutylammoniun hexafluorophosphate ($n\text{-}Bu_4NPF_6$) in DCM as electrolyte; Ag/0.01 M $AgNO_3$ electrode (acetonitrile as solvent) as the reference electrode; a glassy carbon disk (diameter 3 mm) as the working electrode; a platinum wire as the counter electrode. Scan rate: 50 mV/s. All redox potentials were calibrated vs. normal hydrogen electrode (NHE) by the addition of ferrocene. The conversion $E_{(Fc/Fc+)}$ = 630 mV vs NHE was used; [b)]Calculated from the intersection of the normalized absorption and emission spectra (Figure 2a); [c)]E_R: reorganization energy, calculated using the four-point method based on the adiabatic potential energy surface; [d)]Pure HTM without doping; [e)]**X19** and **X51** doped with 30 mM LiTFSI, Spiro-OMeTAD doped with 20 mM LiTFSI.

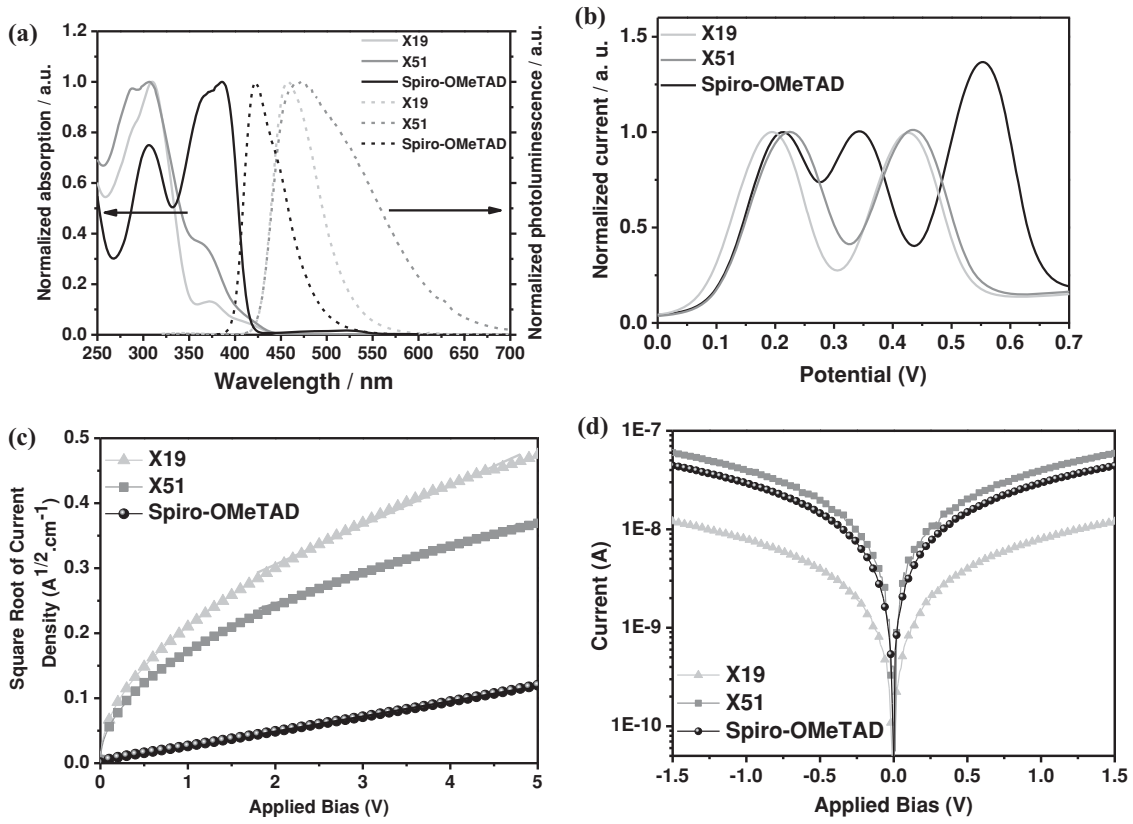

Figure 2. (a) Normalized UV-Visible absorption and photoluminescence of **X19** and **X51** in DCM (10^{-5} M). (b) Normalized differential pulsed voltammetry (DPV) of **X19, X51** and Spiro-OMeTAD in DCM (10^{-4} M). (c) *J–V* characteristic of thin films in hole-conducting only devices. (d) Current-voltage characteristics of different HTM films after LiTFSI-doping.

both of these carbazole-based HTMs showed almost three times higher hole mobility than of Spiro-OMeTAD. These results are in good agreement with the implications from the computational data showing that the molecule **X51** has the lowest calculated reorganization energy. The conductivities of the films were determined by using a two-contact electrical conductivity set-up, which were performed by following a published procedure. The curves obtained and values recorded for the LiTFSI-doped HTMs are depicted in Figure 2d and Table 1. The conductivity of pure Spiro-OMeTAD closely matches that reported in the literature.[11,20] We note that the conductivity of **X51** is slightly higher than that of Spiro-OMeTAD, but much higher than that of **X19**. This might linked to the larger conjugated system in the former molecular material, leading to more efficient π–π stacking in HTMs films. In this case, the hole mobility and conductivity of **X51** are superior to those of **X19**. Consequently, it is a realistic assumption that the hole transfer of the HTM **X51** could contribute to the better photovoltaic parameters observed as compared to those of **X19-**, as well as Spiro-OMeTAD-based devices; as will discussed in more detail later.

The photovoltaic properties of these HTMs were investigated by fabricating ssDSCs using the organic dye LEG4 known to possess a high molar extinction coefficient. In order to properly evaluate the photovoltaic properties, devices containing Spiro-OMeTAD as HTM were used as reference. It has been widely demonstrated that lithium bis(trifluoromethanesulfonyl) imide (LiTFSI) is essential in ssDSCs to render a low series resistances and to facilitate photocurrent generation.[20,22] Our previous work has also manifested that different HTMs need different concentration of Li^+ doping.[9] Therefore, we firstly optimized the amount of LiTFSI that was added into the HTM solutions used for spin coating. The final optimal Li^+ concentration used for **X19-** and **X51**-based ssDSCs was 30 mM; for *J–V* curves and photovoltaic parameters obtained at different concentrations of LiTFSI doping, see Figure S9 and Table S2. The optimal concentration of LiTFSI used in combination with Spiro-OMeTAD was found to be 20 mM; the same as frequently reported in literature. The *J–V* curves of the best devices containing different HTMs are shown in **Figure 3**a, and the corresponding parameters are stated in **Table 2**. The **X51**-based devices yielded the highest efficiency among these HTMs, up to 6.0%, with a short-circuit photocurrent density (J_{SC}) of 9.27 mA·cm^{-2}, an open-circuit photovoltage (V_{OC}) of 0.92 V and a fill factor (FF) of 0.70. Under the optimal conditions, the **X19**-based devices offered a lower efficiency, 4.5%, with a V_{OC} of 0.75 V, a J_{SC} of 9.62 mA·cm^{-2} and an FF of 0.62. The standard HTM Spiro-OMeTAD-based devices reached a reference efficiency of 5.5% with a V_{OC} of 0.90 V, a J_{SC} of 9.22 mA•cm^{-2} and an FF of 0.66. We can note that the photocurrent densities in all the devices are very similar after optimization of the concentration of LiTFSI. The incident photon-to-current conversion efficiency (IPCE) spectra of these homologous devices are shown in Figure 2b. For the sensitizer used in this study, LEG4, all the HTMs generate highly similar IPCE of 65% at

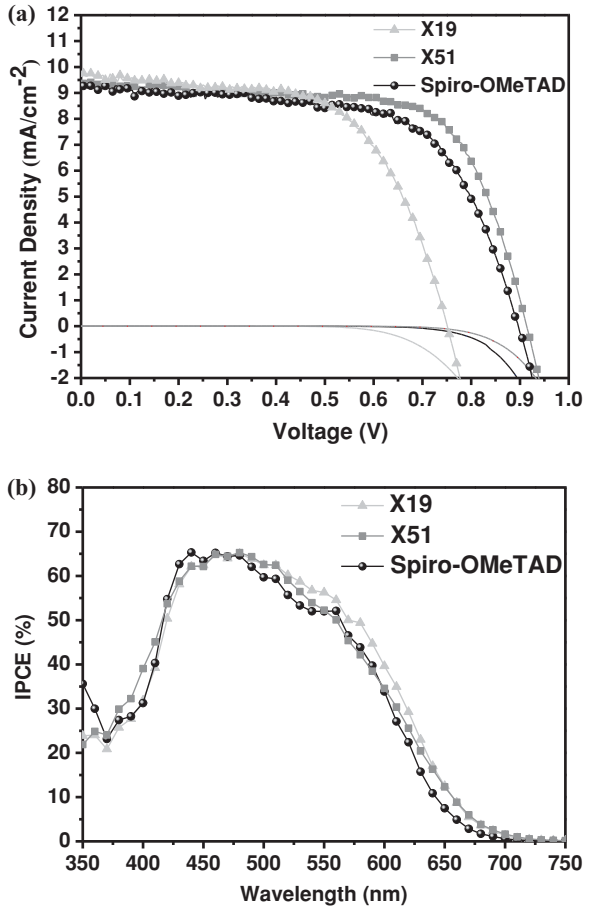

Figure 3. (a) *J–V* characteristics of **X19-**, **X51-** and Spiro-OMeTAD-based ssDSCs studied under 100 mW•cm^{-2} AM1.5G solar illumination, (b) Corresponding IPCE spectra of the devices.

the maximum absorption wavelength of 475 nm. However, the open-circuit voltage of the **X19**-based devices was 170 mV and 150 mV lower than that of the Spiro-OMeTAD- and **X51**-based devices, respectively. One reason may be that the HOMO energies of **X51** and Spiro-OMeTAD are more positive than that of **X19**; another factor might be due to the smaller molecular size of **X19** induces faster electron recombination in the device, an explanation was proposed in our former work.[21] Figure S11 show the τ_e plotted vs. V_{OC} from transient photovoltage decay measurements of these devices. At a certain V_{OC} value, the τ_e values from **X51**-based device was obviously the highest among all of the HTMs (indicating the slowest recombination). Especially, the τ_e value for the **X19**-based device were much lower than that of **X51** and Spiro-OMeTAD-based devices, which is in good agreement with our previous discovery[21] that the HTM-**X19** with small molecule size results in a facilitated approach to the TiO_2 interface, leading to a fast recombination process in the devices.

Table 2. Photovoltaic parameters determined from *J–V* measurements of ssDSCs based on the HTMs. The results were obtained under simulated AM1.5G solar illumination (100 mW·cm^{-2}).

Photosensitizer	HTMs	V_{OC} [V]	J_{SC} [mA·cm^{-2}]	FF	η [%]
	X19[b]	0.75	9.62	0.62	4.5
LEG4[a]	**X51**[c]	0.92	9.27	0.70	6.0
	Spiro-OMeTAD[d]	0.90	9.22	0.66	5.5
	X19[f]	0.76	17.14	0.58	7.6
Perovskite[e]	**X51**[g]	0.88	16.79	0.66	9.8
	Spiro-OMeTAD[h]	0.83	16.82	0.73	10.2

[a]2.0 μm TiO_2 film; [b]180 mM HTM doped with 200 mM t-BP and 30 mM LiTFSI; [c]90 mM HTM doped with 200 mM t-BP and 30 mM LiTFSI; [d]150 mM HTM doped with 200 mM t-BP and 20 mM LiTFSI; [e]350 nm TiO_2 film; [f]120 mM HTM doped with 200 mM t-BP and 30 mM LiTFSI; [g]60 mM HTM doped with 200 mM t-BP and 30 mM LiTFSI; [h]70 mM HTM doped with 200 mM t-BP and 20 mM LiTFSI.

Subsequently, we also fabricated devices based on the HTMs using perovskite as light-harvesting material under the same preparation conditions as used before without any further device optimization; thus, the concentrations of LiTFSI and t-BP were the same as of the ones used for the ssDSC devices. The configuration of this typical solid-state mesoscopic solar cell is as follows: compact TiO_2/nc-TiO_2/$CH_3NH_3PbI_{3-X}Cl_X$/HTM/Ag. A 350 nm thick nc-TiO_2 layer was deposited by spin-coating of a diluted paste, and $CH_3NH_3PbI_{3-X}Cl_X$ was employed as the light harvesting material in virtue of the long electron-hole diffusion lengths in the mixed halide perovskite.[23] The *J–V* curves obtained from the best performing solar cells are showed in **Figure 4**a, and the corresponding photovoltaic parameters are summarized in Table 2. The devices prepared containing Spiro-OMeTAD exhibited the highest conversion efficiency of 10.2%, with a V_{OC} of 0.83 V, a J_{SC} of 16.82 mA·cm^{-2}, and an FF of 0.73, while **X51**-based devices gave rise to an essentially comparable conversion efficiency of 9.8%, with a V_{OC} of 0.88 V, a J_{SC} of 16.79 mA·cm^{-2}, and an FF of 0.66. The devices prepared with **X19** as HTM yielded slightly lower energy output in the form of a V_{OC} of 0.76 V, a J_{SC} of 17.14 mA·cm^{-2}, and an FF of 0.58, giving rise to a PCE of 7.6%, which is lower than the output from the devices prepared with the other HTMs of this study. In addition, we performed a comparative investigation using a higher concentration of LiTFSI (30 mM) doping in the Spiro-OMeTAD solution; however no significant change in conversion efficiency could be detected. The *J–V* curves and photovoltaic parameters obtained from DSCs prepared from HTM solutions containing different concentrations of LiTFSI doping are shown in Figure S10 and Table S2. It was also confirmed that the J_{SC} values of the best performing devices are highly consistent with the results obtained from the IPCE measurements (Figure 4b). However, significant deviations were observed for the V_{OC} and fill factor, where **X51**-based devices exhibited the highest V_{OC} in agreement with the high HOMO energy level of **X51**. Moreover, the fill factor of devices based on **X51** and Spiro-OMeTAD both in ssDSCs and perovskite solar cells were considerably higher than devices made with **X19**, which might cause by the higher conductivity of the former materials resulting in a lower overall device serial resistance.

In conclusion, we have designed and synthesized two new carbozle-based, small molecules, organic HTMs of different molecular weight, oxidation potential, hole mobility, and electrical conductivity. Theoretical studies show that **X51** clearly exhibits a lower reorganization energy implying faster

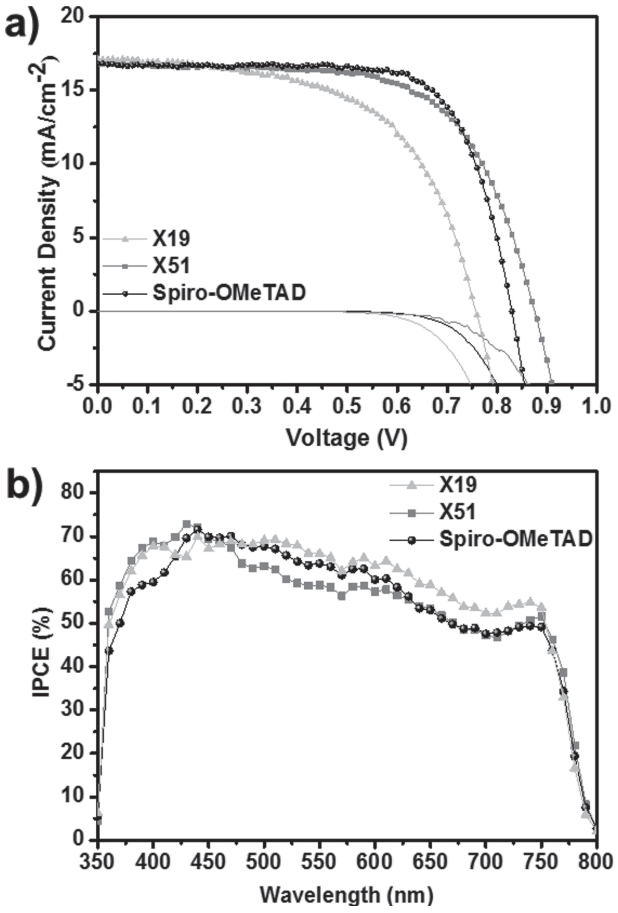

Figure 4. (a) *J–V* characteristics of **X19-**, **X51-** and Spiro-OMeTAD-based perovskite solar cells investigated under 100 mW•cm^{-2} AM1.5G solar illumination. (b) Corresponding IPCE spectra of the devices.

hole transport than **X19**. This is in good agreement with the expected influence of a larger conjugation system in the HTM **X51**.

By optimization of the conduction parameters of the HTMs and subsequent application in ssDSCs using LEG4 as photosensitizer, devices with the HTM **X51** exhibit higher power conversion efficiencies (PCEs) of 6.0% than devices consisting of the smaller HTM **X19** (4.5%). Devices based on the HTM **X51** thus clearly outperform the state-of-the-art HTM Spiro-OMeTAD offering a PCE of 5.5%. Employing perovskite as light-harvesting material, devices containing the HTM **X51** exhibited a higher power conversion efficiency (PCEs) of 9.8%, than that of devices based on the HTM **X19** (7.6%), also comparable to the PCE of 10.2% obtained in devices based on the HTM Spiro-OMeTAD. These results clearly qualify the new family of HTMs as promising future materials for high-efficiency ssDSCs and PSCs. Moreover, **X51** exhibits higher hole mobility and conductivity than **X19**, leading to better photovoltaic performance of the devices investigated. The results obtained show that the use of molecular engineering to develop new and efficient HTMs with high hole mobility and high conductivity is a feasible strategy for the ssDSCs and PSCs in the future.

Supporting Information

Supporting Information is available from the Wiley Online Library or from the author. Scheme S1: The synthetic routes of **X19** and **X51**; Figure S1: Frontier orbitals of the HTMs; Figure S2–S7: Characterization of the new HTMs **X19** and **X51** (^{1}H/^{13}C NMR spectroscopy and HR Mass spectrometry); Figure S8: Cyclic Voltammograms; Figure S9: *J–V* curves of ssDSCs devices containing the HTMs with different concentrations of LiTSFI; Figure S10: *J–V* curves of perovskite solar cells containing Spiro-OMeTAD prepared using different solution concentrations of LiTSFI; Figure S11: Electron lifetime plots of ssDSCs based on different HTMs; Table S1: Calculated electrochemical properties of the HTMs; Table S2: Photovoltaic parameters determined from *J–V* measurements of ssDSCs and perovskite solar cells at different LiTFSI doping levels.

Acknowledgements

This work was financially supported by the Swedish Research Council, the Swedish Energy Agency, the Knut and Alice Wallenberg Foundation, the National Natural Science Foundation of China (21120102036, 91233201), the National Basic Research Program of China (973 program, 2014CB239402) and the China Scholarship Council (CSC). We would like to thank Jianghua Zhao (Dalian University of Technology) for recording the HR-MS spectra. We also greatly thank Erik Gabrielsson (KTH) and Jing Huang (KTH) for their helpful discussions and Majid Safdari (KTH) for his kind help in laboratory experiments.

Received: May 30, 2014
Revised: July 4, 2014
Published online: August 15, 2014

[1] a) B. O'Regan, M. Gratzel, *Nature* **1991**, *353*, 737; b) A. Hagfeldt, G. Boschloo, L. Sun, L. Kloo, H. Pettersson, *Chem. Rev.* **2010**, *110*, 6595.
[2] a) H. Tian, L. Sun, *J. Mater. Chem* **2011**, *21*, 10592; b) C.-Y. Hsu, Y.-C. Chen, R. Y.-Y. Lin, K.-C. Ho, J. T. Lin, *Phys. Chem. Chem. Phys.* **2012**, *14*, 14099; c) M. Wang, C. Gratzel, S. M. Zakeeruddin, M. Gratzel, *Energy Environ. Sci.* **2012**, *5*, 9394.
[3] Z. Ning, Y. Fu, H. Tian, *Energy Environ. Sci.* **2010**, *3*, 1170.
[4] a) A. Yella, H.-W. Lee, H. N. Tsao, C. Yi, A. K. Chandiran, M. K. Nazeeruddin, E. W.-G. Diau, C.-Y. Yeh, S. M. Zakeeruddin, M. Grätzel, *Science* **2011**, *334*, 629; b) S. Mathew, A. Yella, P. Gao, R. Humphry-Baker, F. E. CurchodBasile, N. Ashari-Astani, I. Tavernelli, U. Rothlisberger, K. NazeeruddinMd, M. Grätzel, *Nat. Chem.* **2014**, *6*, 242.
[5] U. Bach, D. Lupo, P. Comte, J. E. Moser, F. Weissortel, J. Salbeck, H. Spreitzer, M. Gratzel, *Nature* **1998**, *395*, 583.
[6] P. Docampo, S. Guldin, T. Leijtens, N. K. Noel, U. Steiner, H. J. Snaith, *Adv. Mater.* **2014**, *26*, 4013
[7] J. Burschka, A. Dualeh, F. Kessler, E. Baranoff, N.-L. Cevey-Ha, C. Yi, M. K. Nazeeruddin, M. Grätzel, *J. Am. Chem. Soc.* **2011**, *133*, 18042.
[8] a) H.-S. Kim, C.-R. Lee, J.-H. Im, K.-B. Lee, T. Moehl, A. Marchioro, S.-J. Moon, R. Humphry-Baker, J.-H. Yum, J. E. Moser, M. Gratzel, N.-G. Park, *Sci. Rep.* **2012**, *2*, 591; b) M. M. Lee, J. Teuscher, T. Miyasaka, T. N. Murakami, H. J. Snaith, *Science* **2012**, *338*, 643; c) J. Burschka, N. Pellet, S.-J. Moon, R. Humphry-Baker, P. Gao, M. K. Nazeeruddin, M. Gratzel, *Nature* **2013**, *499*, 316.
[9] B. Xu, H. Tian, D. Bi, E. Gabrielsson, E. M. J. Johansson, G. Boschloo, A. Hagfeldt, L. Sun, *J. Mater. Chem. A.* **2013**, *1*, 14467.
[10] J. Bandara, H. Weerasinghe, *Sol. Energy Mater. Sol. Cells.* **2005**, *85*, 385.

[11] T. Leijtens, I. K. Ding, T. Giovenzana, J. T. Bloking, M. D. McGehee, A. Sellinger, *ACS Nano* **2012**, *6*, 1455.
[12] a) L. Yang, B. Xu, D. Bi, H. Tian, G. Boschloo, L. Sun, A. Hagfeldt, E. M. J. Johansson, *J. Am. Chem. Soc.* **2013**, *135*, 7378; b) M. Planells, A. Abate, D. J. Hollman, S. D. Stranks, V. Bharti, J. Gaur, D. Mohanty, S. Chand, H. J. Snaith, N. Robertson, *J. Mater. Chem. A.* **2013**, *1*, 6949; c) D. Bi, L. Yang, G. Boschloo, A. Hagfeldt, E. M. J. Johansson, *J. Phys. Chem. Lett.* **2013**, *4*, 1532; d) L. Yang, J. Zhang, Y. Shen, B.-W. Park, D. Bi, L. Häggman, E. M. J. Johansson, G. Boschloo, A. Hagfeldt, N. Vlachopoulos, A. Snedden, L. Kloo, A. Jarboui, A. Chams, C. Perruchot, M. Jouini, *J. Phys. Chem. Lett.* **2013**, *4*, 4026.
[13] H. Li, K. Fu, A. Hagfeldt, M. Grätzel, S. G. Mhaisalkar, A. C. Grimsdale, *Angew. Chem. Int. Ed.* **2014**, *53*, 4085.
[14] a) I. Y. Song, S.-H. Park, J. Lim, Y. S. Kwon, T. Park, *Chem. Commun.* **2011**, *47*, 10395; b) I. Chung, B. Lee, J. He, R. P. H. Chang, M. G. Kanatzidis, *Nature* **2012**, *485*, 486; c) J. E. Kroeze, N. Hirata, L. Schmidt-Mende, C. Orizu, S. D. Ogier, K. Carr, M. Grätzel, J. R. Durrant, *Adv. Funct. Mater.* **2006**, *16*, 1832; d) N. J. Jeon, J. Lee, J. H. Noh, M. K. Nazeeruddin, M. Grätzel, S. I. Seok, *J. Am. Chem. Soc.* **2013**, *135*, 19087.
[15] a) A. W. Schmidt, K. R. Reddy, H.-J. Knölker, *Chem. Rev.* **2012**, *112*, 3193; b) G. Puckyte, B. Schmaltz, A. Tomkeviciene, M. Degbia, J. V. Grazulevicius, H. Melhem, J. Bouclé, F. Tran-Van, *J. Power. Sources.* **2013**, *233*, 86.
[16] a) A. Michaleviciute, E. Gurskyte, D. Y. Volyniuk, V. V. Cherpak, G. Sini, P. Y. Stakhira, J. V. Grazulevicius, *J. Phys. Chem. C.* **2012**, *116*, 20769; b) S.-i. Kato, H. Noguchi, A. Kobayashi, T. Yoshihara, S. Tobita, Y. Nakamura, *J. Org. Chem.* **2012**, *77*, 9120.
[17] A. Venkateswararao, K. R. J. Thomas, C.-P. Lee, C.-T. Li, K.-C. Ho, *ACS Appl. Mater. Interfaces.* **2014**, *6*, 2528.
[18] N. Prachumrak, S. Pojanasopa, S. Namuangruk, T. Kaewin, S. Jungsuttiwong, T. Sudyoadsuk, V. Promarak, *ACS Appl. Mater. Interfaces.* **2013**, *5*, 8694.
[19] E. Gabrielsson, H. Ellis, S. Feldt, H. Tian, G. Boschloo, A. Hagfeldt, L. Sun, *Adv. Energy. Mater.* **2013**, *3*, 1647.
[20] H. J. Snaith, M. Gratzel, *Appl. Phys. Lett.* **2006**, *89*, 262114.
[21] B. Xu, H. Tian, L. Lin, D. Qian, H. Chen, J. Zhang, N. Vlachopoulos, G. Boschloo, Y. Luo, F. Zhang, A. Hagfeldt, L. Sun, unpublished.
[22] I. A. Howard, M. Meister, B. Baumeier, H. Wonneberger, N. Pschirer, R. Sens, I. Bruder, C. Li, K. Müllen, D. Andrienko, F. Laquai, *Adv. Energy. Mater.* **2014**, *4*, 1300640.
[23] S. D. Stranks, G. E. Eperon, G. Grancini, C. Menelaou, M. J. P. Alcocer, T. Leijtens, L. M. Herz, A. Petrozza, H. J. Snaith, *Science* **2013**, *342*, 341.